Physics Letters A 384 (2020) 126215

Contents lists available at ScienceDirect

Physics Letters A

www.elsevier.com/locate/pla

The spin-dependent transport properties of endohedral transition-metal-fullerene X@$C_{66}H_4$ (X=Fe, Co, Mn, Ni)

Jian-Hua Li [a,b], Yan-Dong Guo [a,b,*], Hong-Li Zeng [c], Jing-Jing He [a], Yang Ni [a], Qiao-An Li [a], Xiao-Hong Yan [a,b,d,e,*]

[a] College of Electronic and Optical Engineering, Nanjing University of Posts and Telecommunications, Nanjing 210023, China
[b] Key Laboratory of Radio Frequency and Micro-Nano Electronics of Jiangsu Province, Nanjing 210023, China
[c] College of Natural Science, Nanjing University of Posts and Telecommunications, Nanjing 210023, China
[d] College of Science, Nanjing University of Aeronautics and Astronautics, Nanjing 210016, China
[e] School of Material Science and Engineering, Jiangsu University, Zhenjiang, 212013, China

ARTICLE INFO

Article history:
Received 2 August 2019
Received in revised form 3 December 2019
Accepted 20 December 2019
Available online 6 January 2020
Communicated by R. Wu

Keywords:
Endohedral metallofullerenes (EMFs)
Density functional theory (DFT)
Nonequilibrium Greens function (NEGF)
Spin-dependent transport

ABSTRACT

Inspired by recent experiments on the successful synthesis of hydrofullerene $C_{66}H_4$ in Tian et al. (2019) [12] with two negatively curved heptagons. Based on the density functional theory and nonequilibrium Green's function method, we report the spin-dependent transport through transition-metal-atom-encapsulated $C_{66}H_4$ hydrofullerene, i.e., X@$C_{66}H_4$(X=Fe, Co, Mn, Ni), contacted by single gold atoms via semi-infinite non-magnetic Au electrodes. It is found that, Mn- and Fe-doped systems show highly spin-polarized transmission as well as considerable magnetic moments whereas Ni-doped systems show completely spin-unpolarized transmission and nonmagnetic. Interestingly, Co-doped systems show two spin states, i.e., spin-polarized and spin-unpolarized ones. Further analysis shows that, for Mn-, Fe- and Ni-doped systems, the spin-polarized/unpolarized state is caused by the finite/(nearly-)zero magnetism of the encapsulated metal atom. While the magnetism in Co-doped systems is quenched for the top hexagonal doping case, but not for the side heptagonal doping one, which induces the spin-unpolarized/spin-polarized state. And the screening effect of electrodes on the magnetism of Co is the underlying physical mechanism. Our findings would be beneficial to the design of spintronics devices.

1. Introduction

In recent years, fullerenes have attracted extensive interests for next-generation spintronic applications due to their spin-related features, such as spin transistors, spin light-emitting diodes and spin filters [1–5]. Since the discovery of the first buckminsterfullerene (C_{60}) [6], extensive studies on fullerenes have been carried out, e.g., C_{70}, C_{80}, and their endohedral metallofullerenes(EMFs) [7–10]. Particularly, EMFs, as a novel form of fullerene-based materials, have also aroused significant interests. Due to the charge transfer between the encapsulated metal atoms and the fullerene cage, such a kind of molecules open up many possibilities for studies [9–11]. Very recently, Tian et al. [12]. reported the experimental evidence for the existence of an unprecedented hydrofullerene $C_{66}H_4$, which does not satisfy the empirical isolated pentagon rule (IPR) [13,14]. The $C_{66}H_4$ cage with the D_{2v} symmetry possesses nineteen hexagons, fourteen pentagon and two negative curvature heptagons, which differs from all the previously reported fullerenes [15]. Such a new geometric structure is expected to exhibit interesting electronic features, especially the spin-dependent transport properties used for spintronic devices. As is well known, one of the key issues in spintronics is the manipulation of a spin current. Previous studies have shown that magnetic atoms embedded in fullerenes or carbon nanotubes (CNTs) can modulate the electron transport properties [16–19]. However, the spin-dependent electron transport properties of endohedral transition-metal-fullerene X@$C_{66}H_4$ is still lack of study. And there is considerable interest in the magnetic-atom-encapsulated $C_{66}H_4$ hydrofullerene.

In the present work, using the density functional theory (DFT) combined with nonequilibrium Green's function (NEGF), we focus on the spin-dependent electronic transport of endohedral transition-metal-fullerene X@$C_{66}H_4$ (X=Fe, Co, Mn, Ni) under ferromagnetic state (FM), contacted by single gold atoms via semi-

* Corresponding authors.
E-mail addresses: yandongguo@njupt.edu.cn (Y.-D. Guo), yanxh@njupt.edu.cn (X.-H. Yan).

https://doi.org/10.1016/j.physleta.2019.126215
0375-9601/

infinite non-magnetic Au electrodes. Considering the symmetry and the negative curvature fragment of $C_{66}H_4$, the top hexagon and side heptagon holes of $C_{66}H_4$ are suitable candidates to trap magnetic atoms [20]. Therefore, in this work, we focus the studies on these two hole sites for doping transition metal atoms. One finds that Mn- and Fe-doped systems exhibit highly spin-polarized transmission, whereas Ni-doped systems show completely spin-unpolarized transmission. Interestingly, Co-encapsulated systems show two spin states, i.e., spin-polarized and spin-unpolarized ones. Through further investigations, one finds that the spin-polarized/unpolarized state is caused by the finite/(nearly-)zero magnetic moment in Mn-, Fe- and Ni-doped systems. For Co-doped systems, the screening effect of the electrodes on the magnetism of the Co atom induces the spin-unpolarized state. Our findings may throw light on the development of future C-based spintronic nanodevices.

2. Computational method

To explore the electron transport properties of the endohedral transition-metal-fullerene $M@C_{66}H_4$ system, the first-principles method based on DFT coupled with NEGF is implemented, through the Atomistix Toolkit package [21–23]. The electron exchange-correlation function is treated by the Perdew-Burke-Eenzerhof (PBE) formulation of the generalized gradient approximation (GGA) [24,25]. The mesh cutoff energy is set to be 150 Ry, with $1 \times 1 \times 100$ (for the transport calculations) k-point meshes in the Monkhorst-Park scheme. Such the applied cutoff energy and k-point mesh are widely used in the transport investigations, which achieves the calculation efficiency and the accuracy [26–28]. The double-zeta polarized basis set is chosen for the local numerical orbitals. Previous reports [29–32] show that the double-zeta polarized basis set are suitable for transport calculations in the spintronic device. The geometric structures for the metal atom-encapsulated $C_{66}H_4$ are fully optimized until the residual force on each atom is less than 0.02 eV/Å. To eliminate the interactions adjacent layers, sufficient vacuum space of supercell (more than 20 Å) is applied. The distance between electrode surface and molecule is 2.2 and 2.0 Å for the metal atoms on the hollow top hexagon and side heptagon sites, respectively. The electrode-molecule distance is determined by minimizing the total energy of the whole system [33].

In the NEGF scheme, the spin-dependent transmission probability through the two-probe system is calculated by

$$T_{\uparrow/\downarrow}(E) = Tr[\Gamma_L(E)G^R_{\uparrow/\downarrow}(E)\Gamma_R(E)G^A_{\uparrow/\downarrow}(E)], \quad (1)$$

where $G^{A/R}_{\uparrow/\downarrow}(E)$ is the spin-dependent advanced or retarded Green's function for the scattering region (E represents energy), and $\Gamma_{L/R}$ is the coupling matrix between this region and the left/right electrode. $T_{\uparrow/\downarrow}(E)$ represents the probability that an up/down spin electrons with energy E transmits from one electrode to another.

3. Results and discussions

In order to explore spin-dependent electron transport properties of endohedral transition-metal-fullerene, the corresponding two-probe systems are constructed, as shown in Fig. 1. Such a two-probe model consists of three regions, i.e., the central scattering region and semi-infinite left/right electrode. We choose the (001) surface of centered cubic (fcc) Au with a pyramid tip as a left/right electrode to contact with the embedded metal fullerene. For the sake of clarity, a transition metal atom (X) encapsulated in $C_{66}H_4$ is denoted by $X@C_{66}H_4$ (X=Fe, Co, Mn, Ni). Additionally, in our systems, the metal atoms are inside the hydrofullerene $C_{66}H_4$. The Au-$X@C_{66}H_4$-Au refers to the two-probe system coupled with

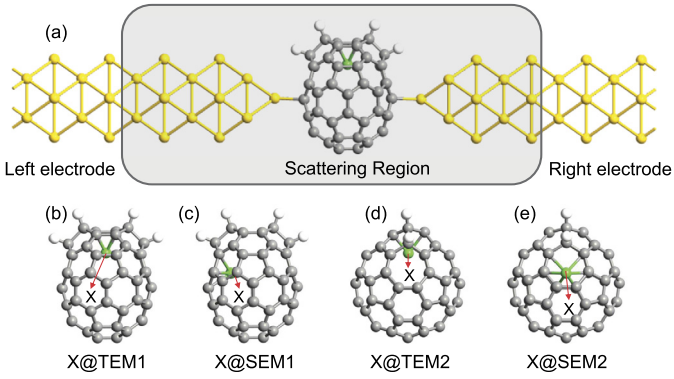

Fig. 1. (a) The schematic plots of the Au-$X@C_{66}H_4$-Au system (X=Fe, Co, Mn, Ni). The X@TEM1 refers to the configuration X-doped on the top hollow hexagon site and the front-contacted with Au electrodes. (b)-(e) The endohedral transition-metal-fullerene part for X@TEM1, X@SEM1, X@TEM2 and X@SEM2, respectively.

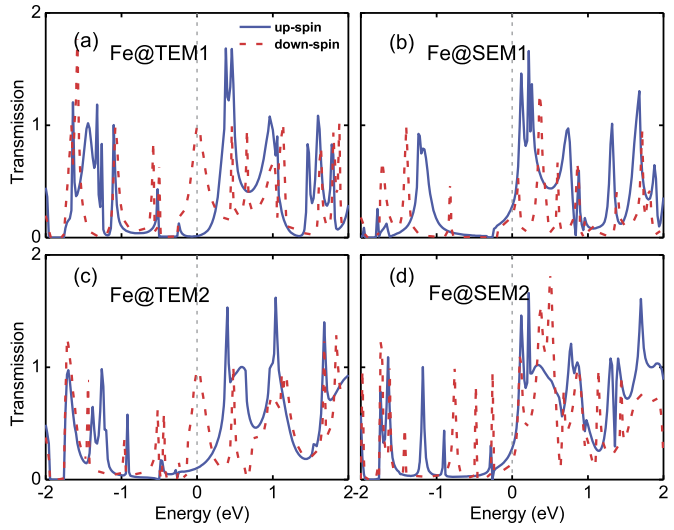

Fig. 2. The transmission spectra for Au-$Fe@C_{66}H_4$-Au system. (a)-(d) Stand for Fe@TEM1, Fe@SEM1, Fe@TEM2 and Fe@SEM2, respectively. The blue solid line denotes the up-spin transmission, and red dashed line denotes down-spin one. The Fermi level (E_F) is set to 0. (For interpretation of the colors in the figure(s), the reader is referred to the web version of this article.)

Au electrodes. Considering the orientation of $C_{66}H_4$ relative to the electrodes, the doping site of the metal atoms and the D_{2v} symmetry of $C_{66}H_4$, we define four kinds of two-probe models, i.e., X@TEM1, X@SEM1, X@TEM2 and X@SEM2, respectively (herein, we only present the endohedral transition-metal-fullerene part), as shown in Fig. 1(b)-(e). For example, the X@TEM1 stands for the configuration where the X atom is doped on the top hollow hexagonal site of $C_{66}H_4$ and the front-contacted with Au electrodes, see Fig. 1(a). It is well known that the transport properties are primarily dependent on transmission around E_F, especially for low-bias conditions, and we focus on transmissions within this energy range. As the ferromagnetic (FM) state could be easily stabilized in experiment, we limit our work to this state in the present work [34].

For Fe-doped systems, the spin-resolved transmission are calculated and plotted in Fig. 2(a)-(d). One finds that, for all the cases, the transmission of up-spin and down-spin are inconsistent. As a result, the electron transmission is spin-polarized. Herein, we define the spin polarization as $[(T_{down} - T_{up})/(T_{down} + T_{up})] \times 100\%$, which is denoted by ξ. Especially, for Fe@TEM1 configuration, there exists a larger down-spin transmission peak around E_F. While the up-spin transmission is much smaller in this energy region, see Fig. 2(a). And the spin polarization has reached as high as

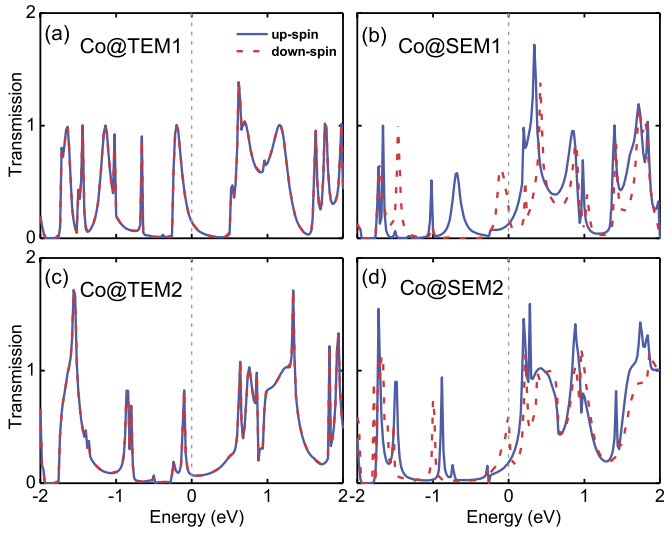

Fig. 3. The transmission spectra for Au-Co@$C_{66}H_4$-Au system. (a)-(d) Stand for Co@TEM1, Co@SEM1, Co@TEM2 and Co@SEM2, respectively. The blue solid line denotes the up-spin transmission, and red dashed line denotes down-spin one. E_F is set to 0.

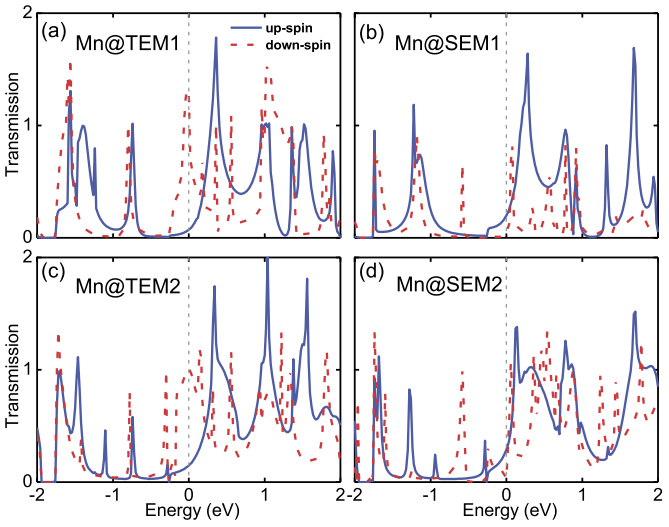

Fig. 4. The transmission spectra for Au-Mn@$C_{66}H_4$-Au system. (a)-(d) Stand for Mn@TEM1, Mn@SEM1, Mn@TEM2 and Mn@SEM2, respectively. The blue solid line denotes the up-spin transmission, and red dashed line denotes down-spin one. E_F is set to 0.

97.2%, which shows great application potential in spintronic devices [35,36]. When we change the orientation of the molecule-electrodes to the Fe@TEM2 configuration, the transmission for the up-spin and down-spin only changes sightly around E_F, see Fig. 2(c). In other words, when the Fe atom is doped on the top hollow hexagonal site, i.e., Fe@TEM1 and Fe@TEM2, the electron transmission of Fe@$C_{66}H_4$ exhibits highly spin polarized transport behavior. However, when the Fe atom is doped on the side hollow heptagonal site, i.e., Fe@SEM1 and Fe@SEM2, the transmissions for the up-spin and down-spin are almost consistent around E_F, see Fig. 2(b) and (d). This means that they are spin-unpolarized. Consequently, the spin polarization of the electron transmission is sensitive to the doping sites and irrelative with the orientation of the molecule-electrodes in Fe-doped systems. One finds that the transition from highly spin-polarized state to spin-unpolarized state could be achieved by modulating the configurations, i.e., from Fe@STM1 to Fe@SEM1, which would facilitate the design of spintronics devices.

Interestingly, Co-doped systems exhibit a strange electron transport behavior. When the Co atom is doped on the top hollow hexagonal sites, i.e., Co@TEM1 and Co@TEM2, the transmissions for up-spin and down-spin are well consistent with each other, including the deep energy regions, see Fig. 3(a) and (c). As a result, they are completely spin-unpolarized (ξ = 0), which is different from the above two cases, i.e., Fe@TEM1 and Fe@TEM2. Particularly, when we change the doping site from the top hollow hexagonal one to the side heptagonal one, i.e., Co@TEM1 and Co@TEM2 to Co@SEM1 and Co@SEM2, respectively, the spin-polarized transmission appears, see Fig. 3(b) and (d). Therefore, the doping site is crucial to the spin-dependent transport in Co-doped systems. Note that, the orientation of the molecule-electrodes has little effect on the spin-dependent transport of Co@$C_{66}H_4$.

For Mn-doped systems, the spin-dependent transmission is calculated and plotted in Fig. 4(a)-(d). One easily finds that, both Mn@TEM1 and Mn@TEM2 systems exhibit highly spin-polarized transmission around E_F, see Fig. 4(a) and (c). And their spin polarization have reached to 89.4% and 74.5%, respectively. However, for Mn@SEM1 and Mn@SEM2, the trends of up-spin and down-spin transmission are the same around E_F, which leads to the spin-unpolarized cases, see Fig. 4(b) and (d). Similar to Fe-encapsulated cases, the configuration-modulated spin polarization effect is also found in Mn-doped systems.

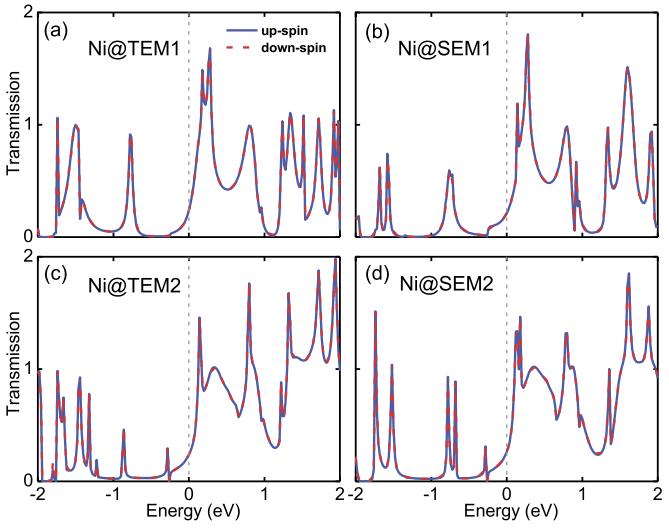

Fig. 5. The transmission spectra for Au-Ni@$C_{66}H_4$-Au system. (a)-(d) Stand for Ni@TEM1, Ni@SEM1, Ni@TEM2 and Ni@SEM2, respectively. The blue solid line denotes the up-spin transmission, and red dashed line denotes down-spin one. E_F is set to 0.

However, for all the Ni-doped in $C_{66}H_4$ cases, the transmission for the up-spin and down-spin remain exactly the same throughout the energy regions of [-2.0, 2.0] eV, see Fig. 5(a)-(d). This means that the transmission for Ni-doped systems are completely spin-unpolarized in the entire energy region (the spin polarization ξ maintains to be 0), which largely differs from Fe-doped and Mn-doped systems, see Fig. 2(a)-(d) and Fig. 4(a)-(d). Meanwhile, these two cases, i.e., Ni@TEM1 and Ni@TEM2, exhibit the same electron transport behavior as Co@TEM1 and Co@TEM2, respectively, see Fig. 4(b), (d) and Fig. 2(b), (d). And they are all completely spin-unpolarized. Moreover, the orientation of the molecule-electrodes and the doping sites in $C_{66}H_4$ have no impact on the spin-polarization of the transport in Ni-doped systems.

To gain insight into the underlying mechanism of spin-dependent transport on endohedral transition metallofullerene X@$C_{66}H_4$, we examine the Mulliken population of metal atoms in the isolated X@$C_{66}H_4$(X=Fe, Co, Mn, and Ni), as shown in Table 1. Herein, the TE and SE denote the metal atom doped on the top hol-

Table 2
The Mulliken population X metal atom in Au-X@$C_{66}H_4$-Au(X=Fe, Co, Mn and Ni) for up-spin, down-spin, and their difference (up-down, i.e., the magnetic moment). The unit of magnetic moment is μ_B.

Structure	X@TEM1			X@SEM1			X@TEM2			X@SEM2		
	↑	↓	↑ − ↓	↑	↓	↑ − ↓	↑	↓	↑ − ↓	↑	↓	↑ − ↓
Fe@$C_{66}H_4$	8.659	6.940	1.719	8.677	6.986	1.691	8.646	6.945	1.701	8.682	6.987	1.695
Co@$C_{66}H_4$	8.244	8.243	0	8.717	7.842	0.875	8.244	8.244	0.001	8.747	7.886	0.861
Mn@$C_{66}H_4$	8.829	5.404	3.425	8.851	5.434	3.417	8.840	5.384	3.456	8.830	5.447	3.383
Ni@$C_{66}H_4$	8.755	8.755	0	8.744	8.743	0.001	8.753	8.753	0	8.760	8.760	0

Table 1
The Mulliken population of X metal atom in isolated X@$C_{66}H_4$(X=Fe, Co, Mn, and Ni), which is not contacted with non-magnetic Au electrodes for up-spin, down-spin, and their difference. Note that the difference (up-down), namely the magnetic moment. The TE and SE represent the metal atom encapsulated on the top hollow hexagonal site and the side heptagonal one of $C_{66}H_4$, respectively. The unit of magnetic moment is μ_B.

Structure	TE			SE		
	↑	↓	↑ − ↓	↑	↓	↑ − ↓
Fe@$C_{66}H_4$	8.745	6.913	1.832	8.781	7.036	1.745
Co@$C_{66}H_4$	8.314	7.349	0.965	8.829	7.871	0.958
Mn@$C_{66}H_4$	8.863	5.346	3.517	8.849	5.370	3.479
Ni@$C_{66}H_4$	8.761	8.760	0.001	8.761	8.760	0.001

low hexagonal site and the side heptagonal one of $C_{66}H_4$, respectively. For the sake of clarity, we define these two cases as TE-X@$C_{66}H_4$ and SE-X@$C_{66}H_4$ respectively. One easily finds that, Fe- and Mn-doped systems show high local magnetic moments, whereas Co-doped systems show low values and Ni-doped systems are completely non-magnetic, see Table 1. It should be noted that the magnetic moments of C and H atoms are almost 0 (here not presented). So, the magnetic moments are actually arisen from doped metal atoms. In other words, doped metal atoms are the origin of magnetism, which is considered as the center of magnetism. As a result, there is no antiferromagnetic (AFM) state in our systems. The magnetic behaviors for transition metal atoms (Fe, Co, Mn and Ni) in our systems are well in agreement with that of transition metal-doped carbon and silicon nanotubes [37, 17,38]. For Fe- or Mn-doped configurations, the magnetic moments of the Fe or Mn atoms are quite large, i.e., 1.832, 1.745, 3.517 and 3.479 μ_B, corresponding to TE-Fe@$C_{66}H_4$, SE-Fe@$C_{66}H_4$, TE-Mn@$C_{66}H_4$ and SE-Mn@$C_{66}H_4$, respectively. These cases exhibit spin-polarized transmission behavior in their two-probe systems, see Fig. 2 and Fig. 4. Whereas Ni-encapsulated configurations, i.e., TE-Ni@$C_{66}H_4$ and SE-Ni@$C_{66}H_4$, are completely nonmagnetic (the magnetic moments are almost 0), and they are spin-unpolarized, see Fig. 5. Consequently, for Fe-, Mn- and Ni-doped configurations, finite/(nearly-)zero magnetic moments of the metal atoms triggers the spin-polarized/unpolarized transmission behavior.

Interestingly, it seems that the rule can not be applied to Co-doped configurations. For Co-doped systems, the magnetic moment of the Co atom in SE-Co@$C_{66}H_4$ is 0.958 μ_B. Although the magnetic moment of Co atom is smaller than that of Fe and Mn in $C_{66}H_4$, it can still result in spin-polarized transmission, see Fig. 3(b) and (d). Compared with SE-Co@$C_{66}H_4$, the Co atom has a larger magnetic moments, i.e., 0.965 μ_B in TE-Co@$C_{66}H_4$, while the corresponding two-probe systems show completely spin-unpolarized transmission, see Fig. 3(a) and (c). It would be interesting to figure out such a transport behavior in Co-doped systems.

In this wok, although the Au electrode is nonmagnetic, it may still have an effect on the transport and magnetic properties of the molecule and then affect the electron transport. In order to confirm that, we explore the Mulliken population of metal atoms in $C_{66}H_4$ coupled with Au electrodes (Au-X@$C_{66}H_4$-Au), as shown in Table 2. One finds that, compared with the isolated Fe- or Mn-doped configurations, the magnetic moments change quite a little in their corresponding two-probe systems (Au-X@$C_{66}H_4$-Au). Considering the orientation of the molecule-electrode, the magnetic moments of Fe atoms become 1.719, 1.701 and 1.691, 1.695 μ_B, corresponding to Fe@TEM1, Fe@TEM2, Fe@SEM1 and Fe@SEM2, respectively. And the magnetic moments of Mn atoms become 3.425, 3.456, 3.417 and 3.383 μ_B, corresponding to Mn@TEM1, Mn@TEM2, Mn@SEM1 and Mn@SEM2, respectively, see Table 2 and Fig. 1. For Ni-doped systems, the magnetic moments of Ni atoms remain still zero (or almost zero) values. This is well consistent with the results of the isolated X@$C_{66}H_4$ molecules. For these cases, Au electrodes have little effect.

In Co-doped two-probe systems, the magnetic moments of Co atoms are 0.875 and 0.861 μ_B for the configurations of Co@SEM1 and Co@SEM2 (see Fig. 1(c) and (e)), respectively. Although the magnetic moments of Co atoms are smaller than that of the isolated SE-Co@$C_{66}H_4$ molecule (0.958 μ_B), they are still non-zero values and can result in the spin-polarized transmission, see Fig. 3(b) and (d). However, for the systems of Co@TEM1 and Co@TEM2 (see Fig. 1(b) and (d)), the magnetic moments of Co atoms become zero (or almost zero), i.e., 0, 0.001 μ_B, respectively. In other words, these magnetic moments are completely quenched compared with that in the isolated TE-Co@$C_{66}H_4$ molecule (0.965 μ_B). Obviously, the coupling between the electrodes and the endohedral transition-metal-fullerene molecule (Co@$C_{66}H_4$) induces different magnetic behaviors for Co atoms. This interesting phenomenon could be seen as screening of the electrodes. Actually, such a screening has been reported before in transition-metal-encapsulated Si cage systems [39]. In those systems, the magnetic moment of the Co atom is screened by the electrodes and becomes completely quenched, but that of Fe and Mn not. Therefore, Co-doped systems exhibit completely spin-unpolarized transmission. While Fe- or Mn-doped systems show highly spin-polarized transmission, which is well in agreement with our systems. Obviously, the screening effect of electrodes is crucial to such Co-doped systems. All in all, the completely spin-unpolarized transmissions of Co@TEM1 and Co@TEM2 are caused by the (almost) zero magnetic moment, see Fig. 3(a) and (c). So, we can draw the conclusion that it is the none-zero/zero magnetic moment in two-probe systems that triggers the spin-polarized/spin-unpolarized transmission.

To better understand the origin of these highly spin-polarized states, we take Fe@TEM1 and Mn@TEM2 (see Fig. 1(a) and (d)) as examples and examine their molecular projected self-consistent Hamiltonian (MPSH) of the two frontier molecular orbitals, i.e., the highest occupied molecular orbital (HOMO), the lowest unoccupied molecular orbital (LUMO) for both spins, respectively, see Fig. 6. Actually, the eigenstates of MPSH could be seen as molecular orbitals renormalized by the molecule-electrode interaction, which intuitively reflects the nature of transport. One easily finds that, for Fe@TEM1 system, the HOMO of down-spin is delocalized throughout the whole two-probe system around E_F, which contributes to a larger transmission for down-spin, see Fig. 6(c) and Fig. 2(a). However, the HOMO and LUMO of up-spin locally distributes on the left and right Au electrodes, indicating that the coupling between molecule and electrodes is very weak, which results in a much smaller transmission for up-spin, see Fig. 6(a), (b) and Fig. 2(a). As a result, the system of Fe@TEM1 shows highly

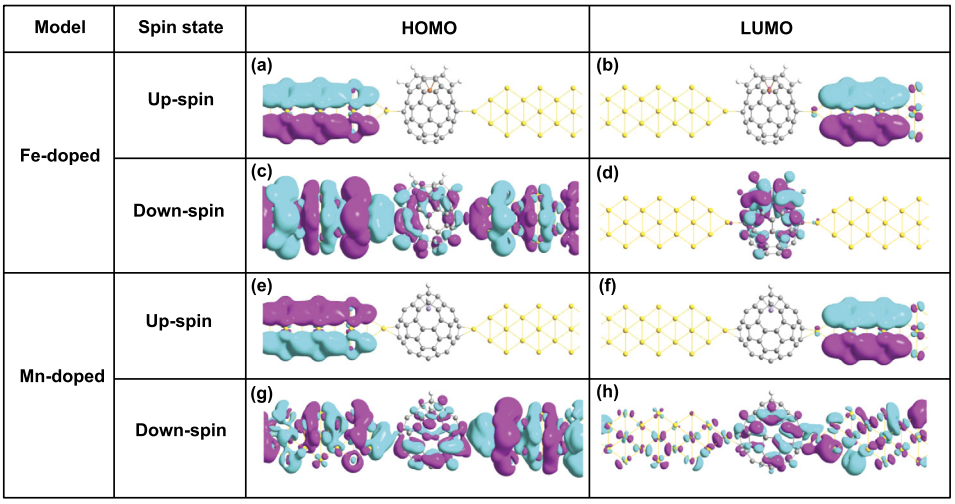

Fig. 6. The spatial HOMO and LUMO states distribution of molecular projected self-consistent Hamiltonian (MPSH) for both spins. (a)-(d) The HOMO and LUMO states of Fe@TEM1 for both spins, respectively. (e)-(h) The HOMO and LUMO states of Mn@TEM2 for both spins, respectively. The isovalue of all the plotted isosurfaces is $0.01e/\text{Å}^3$.

spin-polarized transmission. Meanwhile, a parallel analysis is also performed for Mn@TEM2 system, and the same conclusion can be drawn. Furthermore, to evaluate the stability of this endohedral transition metal fullerene X@$C_{66}H_4$(X=Fe, Co, Mn, and Ni), we computed the cohesive energy of each system. These large cohesive energies (up to 8 eV/atom or more) indicate strongly bonded structure for each system in the present work. In particular, for these two doping configurations, TE- Fe@$C_{66}H_4$ and TE- Co@$C_{66}H_4$, the binding energies of up to 8.43 eV/atom suggests the most possible ones in experiment.

4. Conclusion

In conclusion, we have studied the spin-dependent electron transport properties of endohedral transition-metal-fullerene in $C_{66}H_4$ under first-principles method combined with non-equilibrium Green's function technique. It is found that, Mn- and Fe-doped systems show highly spin-polarized transmission as well as considerable magnetic moments whereas Ni-doped systems show completely spin-unpolarized transmission and nonmagnetic. However, for Co-encapsulated $C_{66}H_4$ systems, the transmission of the top hexagonal hole-doped case is completely spin-unpolarized, but that of the side heptagonal hole-doped one is spin-polarized. Further investigation shows that, for Mn-, Fe- and Ni-doped systems, the spin-polarized/unpolarized state is caused by the finite/(nearly-)zero magnetic moment. And for Co-doped systems, the screening effect of the electrodes is responsible for the spin-unpolarized state. These results are beneficial for spintronics as well as other nanoscale magnetic device applications.

Declaration of competing interest

The authors declare that they have no known competing financial interests or personal relationships that could have appeared to influence the work reported in this paper.

Acknowledgements

This work is supported by the National Natural Science Foundation of China (11504178, 11705097 and 11804158), the Natural Science Foundation of Jiangsu Province (BK20170895), the Scientific Research Foundation of Nanjing University of Posts and Telecommunications (NY217013), Natural Science Found for Colleges and Universities in Jiangsu Province (17KJB140015), the Foundation of New Energy Technology Engineering Laboratory of Jiangsu Province (KF0103), and the Funding of Jiangsu Innovation Program for Graduate Education (SJCX19_0274).

References

[1] M. Ouyang, D.D. Awschalom, Coherent spin transfer between molecularly bridged quantum dots, Science 301 (5636) (2003) 1074–1078.
[2] J. Shim, K. Raman, Y. Park, T. Santos, G. Miao, B. Satpati, J. Moodera, Large spin diffusion length in an amorphous organic semiconductor, Phys. Rev. Lett. 100 (22) (2008) 226603.
[3] I. Žutić, J. Fabian, S.D. Sarma, Spintronics: fundamentals and applications, Rev. Mod. Phys. 76 (2) (2004) 323.
[4] A. Fert, Nobel lecture: origin, development, and future of spintronics, Rev. Mod. Phys. 80 (4) (2008) 1517.
[5] C. Herrmann, G.C. Solomon, M.A. Ratner, Organic radicals as spin filters, J. Am. Chem. Soc. 132 (11) (2010) 3682–3684.
[6] H.W. Kroto, J.R. Heath, S.C. O'Brien, R.F. Curl, R.E. Smalley, C60: buckminsterfullerene, Nature 318 (6042) (1985) 162.
[7] D. McKenzie, C. Davis, D. Cockayne, D. Muller, A. Vassallo, The structure of the C70 molecule, Nature 355 (6361) (1992) 622.
[8] F. Furche, R. Ahlrichs, Fullerene C 80: are there still more isomers, J. Chem. Phys. 114 (23) (2001) 10362–10367.
[9] H. Shinohara, Endohedral metallofullerenes, Rep. Prog. Phys. 63 (6) (2000) 843.
[10] T. Huang, J. Zhao, M. Feng, A.A. Popov, S. Yang, L. Dunsch, H. Petek, A molecular switch based on current-driven rotation of an encapsulated cluster within a fullerene cage, Nano Lett. 11 (12) (2011) 5327–5332.
[11] Y. Yasutake, Z. Shi, T. Okazaki, H. Shinohara, Y. Majima, Single molecular orientation switching of an endohedral metallofullerene, Nano Lett. 5 (6) (2005) 1057–1060.
[12] H. Tian, M. Chen, K. Wang, Z. Chen, C. Fu, Q. Zhang, S. Li, S. Deng, Y. Yao, S. Xie, et al., An unconventional hydrofullerene C66H4 with symmetric heptagons retrieved in low-pressure combustion, J. Am. Chem. Soc. 16 (141) (2019) 6651–6657.
[13] H.W. Kroto, The stability of the fullerenes Cn, with n = 24, 28, 32, 36, 50, 60 and 70, Nature 329 (6139) (1987) 529–531.
[14] K.M. Kadish, R.S. Ruoff, Fullerenes: Chemistry, Physics, and Technology, John Wiley & Sons, 2000.
[15] S.H. Pun, Q. Miao, Toward negatively curved carbons, Acc. Chem. Res. 51 (7) (2018) 1630–1642.
[16] J. Palacios, A. Pérez-Jiménez, E. Louis, J. Vergés, Fullerene-based molecular nanobridges: a first-principles study, Phys. Rev. B 64 (11) (2001) 115411.
[17] C.-K. Yang, J. Zhao, J.P. Lu, Magnetism of transition-metal/carbon-nanotube hybrid structures, Phys. Rev. Lett. 90 (25) (2003) 257203.
[18] C. Li, J. Liu, S. Zhang, G. Lefkidis, W. Hübner, Strain assisted ultrafast spin switching on Co2@ C60 endohedral fullerenes, Carbon 87 (2015) 153–162.
[19] T. Yumura, Y. Sato, K. Suenaga, K. Urita, S. Iijima, Gate effect of vacancy-type defect of fullerene cages on metal-atom migrations in metallofullerenes, Nano Lett. 6 (7) (2006) 1389–1395.
[20] H. Bai, Q. Chen, H. Zhai, S. Li, Endohedral and exohedral metalloborospherenes: M@B40 (M=Ca, Sr) and M@B40 (M=Be, Mg), Angew. Chem., Int. Ed. Engl. 54 (3) (2015) 941–945.

[21] M. Brandbyge, J.-L. Mozos, P. Ordejón, J. Taylor, K. Stokbro, Density-functional method for nonequilibrium electron transport, Phys. Rev. B 65 (16) (2002) 165401.
[22] H. Monkhorst, J. Pack, Special points for Brillouin-zone integrations, Phys. Rev. B 13 (1976) 5188.
[23] M. Paulsson, M. Brandbyge, Transmission eigenchannels from nonequilibrium Green's functions, Phys. Rev. B 76 (11) (2007) 115117.
[24] J.P. Perdew, K. Burke, M. Ernzerhof, Generalized gradient approximation made simple, Phys. Rev. Lett. 77 (18) (1996) 3865.
[25] B. Hammer, L.B. Hansen, J.K. Nørskov, Improved adsorption energetics within density-functional theory using revised Perdew-Burke-Ernzerhof functionals, Phys. Rev. B 59 (11) (1999) 7413.
[26] H.J. Monkhorst, J.D. Pack, Special points for Brillouin-zone integrations, Phys. Rev. B 13 (12) (1976) 5188.
[27] Z. Yu, M. Hu, C. Zhang, C. He, L. Sun, J. Zhong, Transport properties of hybrid zigzag graphene and boron nitride nanoribbons, J. Phys. Chem. C 115 (21) (2011) 10836–10841.
[28] J. Zeng, K.-Q. Chen, Abnormal oscillatory conductance and strong odd–even dependence of a perfect spin-filtering effect in a carbon chain-based spintronic device, J. Mater. Chem. C 3 (22) (2015) 5697–5702.
[29] S. Zhu, T. Li, Strain-induced programmable half-metal and spin-gapless semiconductor in an edge-doped boron nitride nanoribbon, Phys. Rev. B 93 (11) (2016) 115401.
[30] X. Dai, L. Zhang, J. Li, Z. Wang, H. Li, Electronic transport properties of heterojunction devices constructed by single-wall Fe 2 Si and carbon nanotubes, J. Mater. Chem. C 6 (21) (2018) 5794–5802.
[31] Y. Zhou, Y. Li, J. Li, J. Dong, H. Li, Electronic transport properties of carbon and boron nitride chain heterojunctions, J. Mater. Chem. C 5 (5) (2017) 1165–1178.
[32] L. Senapati, J. Schrier, K.B. Whaley, Electronic transport, structure, and energetics of endohedral Gd@ C82 metallofullerenes, Nano Lett. 4 (11) (2004) 2073–2078.
[33] H. Hao, X. Zheng, L. Song, R. Wang, Z. Zeng, Electrostatic spin crossover in a molecular junction of a single-molecule magnet Fe 2, Phys. Rev. Lett. 108 (1) (2012) 017202.
[34] S. Okada, A. Oshiyama, Magnetic ordering in hexagonally bonded sheets with first-row elements, Phys. Rev. Lett. 87 (14) (2001) 146803.
[35] X. Zhang, X. Ai, R. Zhang, Q. Ma, Z. Wang, G. Qin, J. Wang, S. Wang, K. Suzuki, T. Miyazaki, et al., Spin conserved electron transport behaviors in fullerenes (C60 and C70) spin valves, Carbon 106 (2016) 202–207.
[36] T. Koga, J. Nitta, H. Takayanagi, S. Datta, Spin-filter device based on the Rashba effect using a nonmagnetic resonant tunneling diode, Phys. Rev. Lett. 88 (12) (2002) 126601.
[37] Y. Yagi, T.M. Briere, M.H. Sluiter, V. Kumar, A.A. Farajian, Y. Kawazoe, Stable geometries and magnetic properties of single-walled carbon nanotubes doped with 3 d transition metals: a first-principles study, Phys. Rev. B 69 (7) (2004) 075414.
[38] A.K. Singh, T.M. Briere, V. Kumar, Y. Kawazoe, Magnetism in transition-metal-doped silicon nanotubes, Phys. Rev. Lett. 91 (14) (2003) 146802.
[39] L. Kong, J.R. Chelikowsky, Transport properties of transition-metal-encapsulated Si cages, Phys. Rev. B 77 (7) (2008) 073401.